Geophys. J. Int. (1995) **123,** 727–743

The intermediate-wavelength magnetic anomaly maps of the North Atlantic Ocean derived from satellite and shipborne data

Jafar Arkani-Hamed,[1] Jacob Verhoef,[2] Walter Roest[3] and Ron Macnab[2]

[1]*Earth and Planetary Sciences, McGill University, Montreal, Quebec, Canada* H3A 2A7
[2]*Atlantic Geoscience Centre, Geological Survey of Canada, Dartmouth, Nova Scotia, Canada* B2Y 4A2
[3]*Geophysics Division, Geological Survey of Canada, 1 Observatory Crescent, Ottawa, Ontario, Canada* K1A OY3

Accepted 1995 May 5. Received 1995 March 13; in original form 1994 July 15

SUMMARY

Two intermediate-wavelength magnetic anomaly maps of the North Atlantic Ocean are derived based on satellite and marine magnetic observations. The satellite map is produced from the covariant features of POGO and Magsat dawn and Magsat dusk magnetic anomalies. The marine map is compiled using shipborne data collected since 1965. The two maps are in excellent agreement over well-defined anomalies both in location and amplitude, suggesting that these anomalies are real and reflect magnetization contrasts in the oceanic lithosphere. Both maps show the intermediate-wavelength seafloor-spreading anomalies of the Cretaceous quiet zone of the central North Atlantic Ocean as well as the negative seafloor-spreading anomaly of the Labrador Sea caused by dominantly reversed polarity periods. The Iceland hotspot, Alpha Ridge, Azores High, King's Trough and the Rockall microcontinent have positive anomalies. There is no consistent magnetic signature associated with the ocean–continent boundary, although the deep sedimentary basin of Nova Scotia is delineated by a well-defined negative anomaly.

Key words: magnetic anomalies, Magsat, North Atlantic.

INTRODUCTION

Global magnetic anomaly maps of the Earth derived from satellite data (see Arkani-Hamed, Langel & Purucker 1994 and the references cited there) show good correlation over anomalies with amplitudes larger than about 4 nT, suggesting that these anomalies are real and reflect magnetic sources in the lithosphere. The satellite maps, however, show differences over small-scale and low-amplitude anomalies. Although usually minor, these differences throw doubt on the authenticity of the small-scale magnetic anomalies and limit their use in geological studies. Moreover, global maps derived from satellite data usually have a lower resolution than regional maps because data processing on a regional scale can be better controlled.

At a regional scale, a reliable satellite magnetic anomaly map provides a good basis for levelling aeromagnetic and shipborne surveys when compiling continental-size magnetic anomaly maps. For example, the comparison of Magsat anomalies of North America with the upward continued magnetic anomalies compiled from several aeromagnetic maps (Arkani-Hamed & Hinze 1990) demonstrated that the compilation process had introduced significant errors into the intermediate-scale magnetic anomalies, as subsequently demonstrated by Grauch (1993), and thus had compromised the reliability of the compiled data for regional tectonic purposes.

This paper is an attempt to derive regional-scale magnetic anomaly maps of the North Atlantic Ocean using satellite and marine magnetic data. The satellite map is derived from common features of the most recent Magsat and POGO maps selected on the basis of a correlation and covariance analysis. The marine map is compiled using shipborne data available since 1965.

THE SATELLITE MAGNETIC ANOMALY MAP OF THE NORTH ATLANTIC OCEAN

The POGO satellites (OGO-2, OGO-4 and OGO-6) operated from October 1965 to June 1969, acquiring data at latitudes up to 87.3°, at altitudes between 400 and 1510 km, and at all local times and seasons. Recently, Arkani-Hamed *et al.* (1994) used the equivalent source representation of Langel (1990) and determined the POGO scalar magnetic anomalies at 400 km altitude, which were gridded at 0.5° latitude and 0.5° longitude intervals. Fig. 1 portrays a 512 × 512 point grid of the magnetic values on a transverse Mercator projection extracted from the gridded POGO data over the North Atlantic Ocean and adjacent land masses (referred to hereafter as the POGO map).

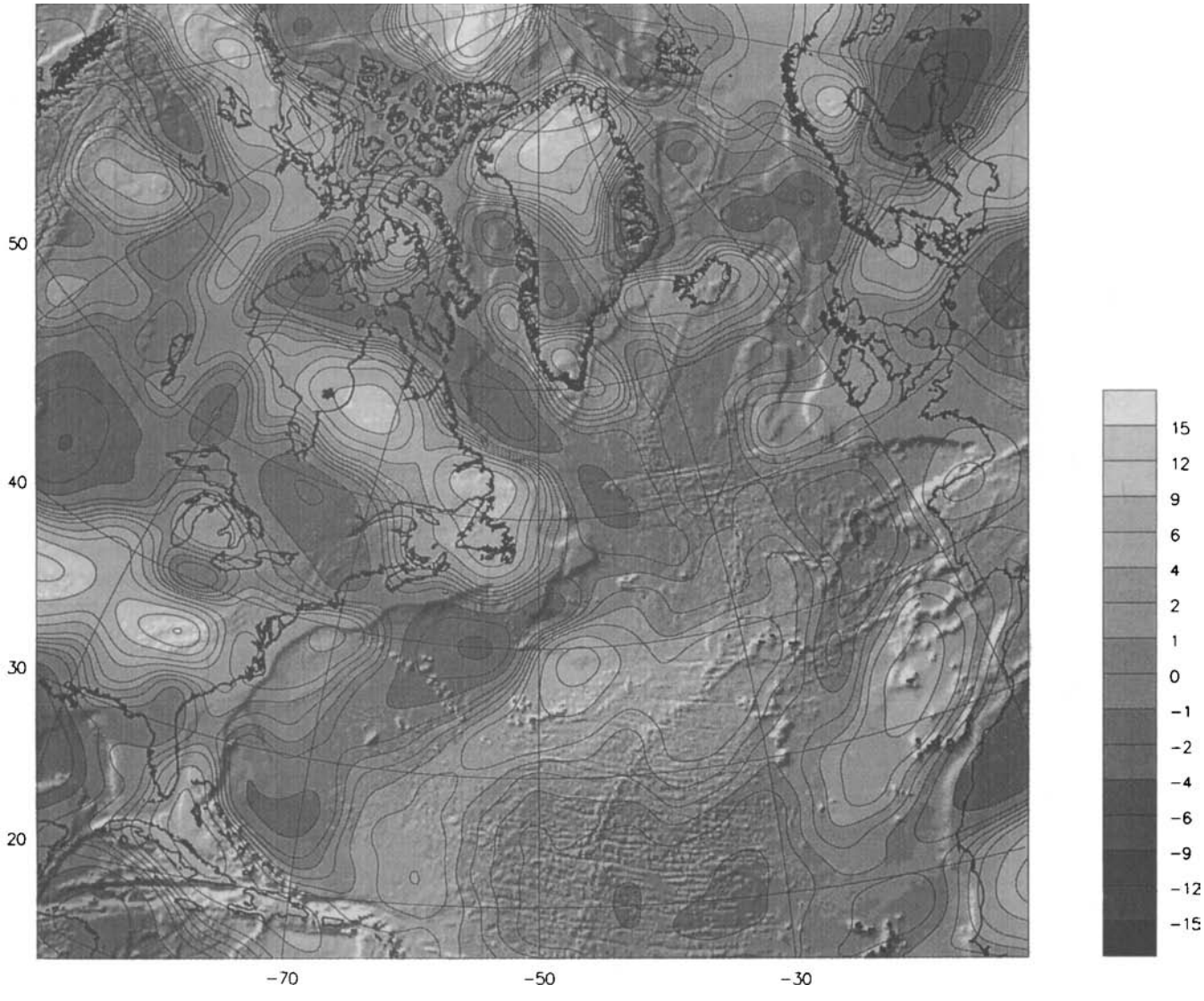

Figure 1. Magnetic anomaly map of the North Atlantic Ocean extracted from the POGO data gridded by Arkani-Hamed *et al.* (1994). A transverse Mercator projection, with a central meridian of 50°W and a non-linear grey scale are used in this map and throughout the paper.

A grid interval of 20 km was selected for this and all other maps presented in this paper. This grid interval is much smaller than that needed for a satellite map: its Nyquist wavelength is only 40 km, which is about an order of magnitude smaller than the wavelength resolution expected for satellite observations at 400 km altitude. We adopted this short interval for the sake of consistency with the marine magnetic anomaly map described later in this paper.

Magsat operated in late 1979 and early 1980 and measured the Earth's magnetic field at altitudes between 350 and 600 km, and at two distinct local times, dawn and dusk. Most recently, Ravat *et al.* (1995) made a determined effort to clean Magsat data using the most appropriate methods developed in the last 15 years by Magsat investigators. After separating the dawn and dusk data and selecting data during magnetic quiet periods, on the basis of planetary activity index (Kp) for low- and mid-latitudes and the auroral electrojet index (AE) for polar regions, they removed the core-field model based on dawn data (Langel & Estes 1985a) from the low- and mid-latitude data and the core-field model based on both dawn and dusk data (Langel & Estes 1985b) from the polar data. The residuals were corrected for the magnetospheric field effects, arising from magnetopause and magnetotail currents and the ring current, by applying a 4000 km wavelength high-pass Kaiser filter (Kaiser 1974). Subsequently, they corrected the data for the effects of the ionospheric currents following the procedure adopted by Ravat & Hinze (1993) and gridded the residuals at 0.5° latitude and 0.5° longitude intervals, resulting in Magsat scalar magnetic anomalies at 400 km altitude. Figs 2(a) and (b) show the Magsat dawn and dusk maps of the North Atlantic Ocean extracted from these gridded data (referred to hereafter as the dawn and dusk maps, respectively).

Fig. 3 displays the energy spectra of these three satellite maps determined by

$$E_K = \sum_{uv} (|F_{u,v}|^2 + |F_{u,-v}|^2), \tag{1}$$

in which $F_{u,v}$ is the Fourier transform of a given magnetic map and u and v are the wavenumbers in the E–W and N–S

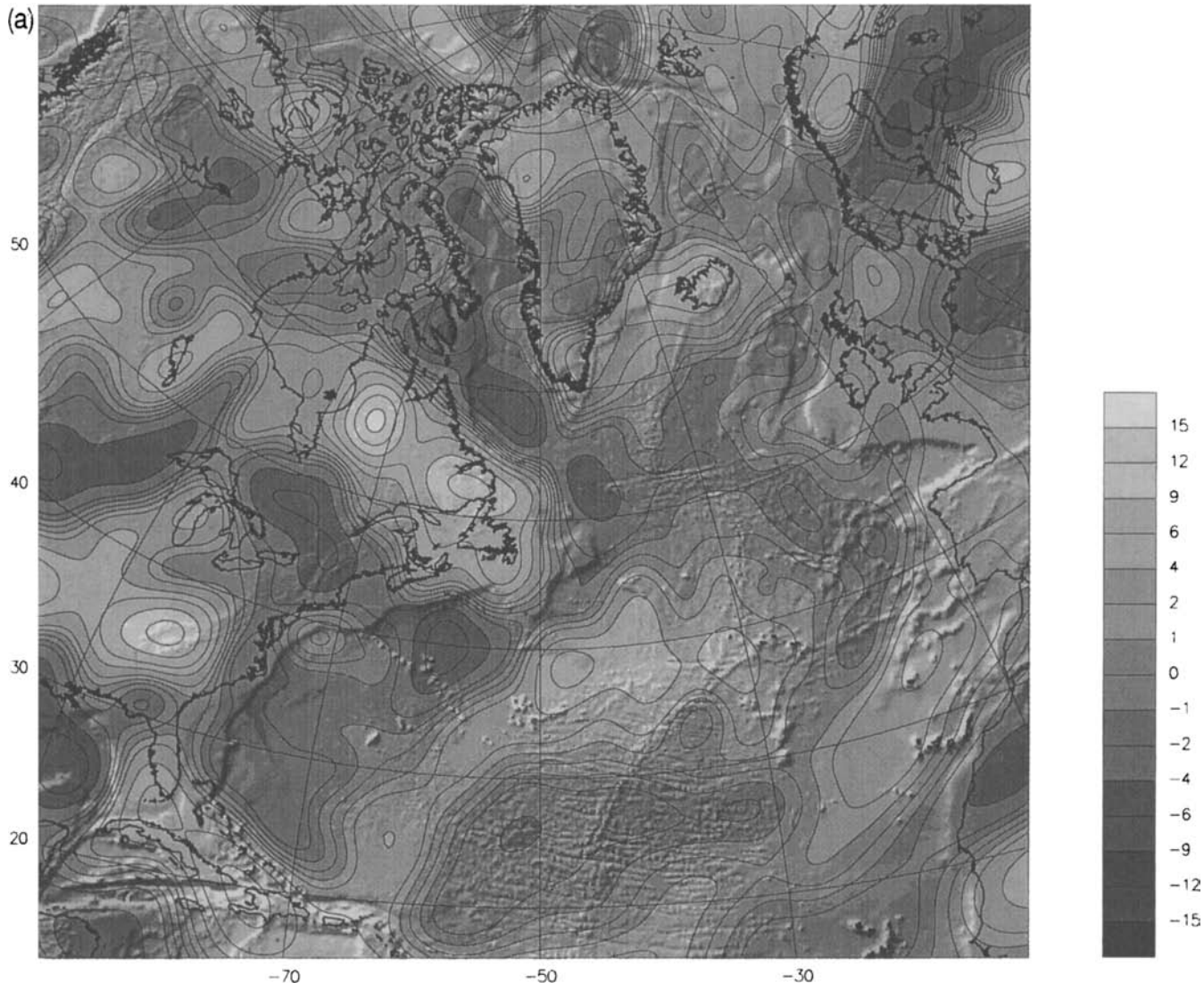

Figure 2. Magnetic anomaly map of the North Atlantic Ocean extracted from the (a) Magsat dawn, and (b) Magsat dusk data gridded by Ravat *et al.* (1995).

directions, respectively. E_K is the total energy of all harmonics with 2-D wavenumbers R_{uv},

$$R_{uv}=\{u^2+v^2\}^{1/2}, \tag{2}$$

between K and $K+1$. The wavelength λ is related to K by

$$\lambda=L/K, \tag{3}$$

where L is the dimension of the map. For example, the fundamental wavelength of the North Atlantic maps is 10240 km ($K=1$) and the Nyquist wavelength is 40 km ($K=256$). The spectra can be divided into three distinct trends. For wavenumbers ≤ 4 (wavelengths longer than 2560 km), the energy increases with the wavenumber. This part of the spectra overlaps the core field, and is affected by the core-field models which were removed from the original measurements in order to extract the satellite magnetic anomalies. The removal of the core-field models has removed parts of the broad-scale magnetic anomalies of the lithosphere. The remaining part is probably not a good representative of the actual anomalies, and is therefore not reliable. Between the wavenumbers 5 and 65 (wavelengths of 2048–157 km), the energy sharply decreases with the increase of the wavenumber, but relatively slowly for the wavenumbers between 29 and 35. There are many reasons to believe that the wavenumbers higher than 29 (wavelengths shorter than 350 km) are substantially contaminated by non-lithospheric sources. The high altitude of the satellite observations (400 km) limits the resolution of the satellite magnetic anomalies to wavelengths comparable to the altitude. The resolution of the global magnetic anomaly maps derived from Magsat data (e.g. Cain *et al.* 1989; Cohen & Achache 1990; Ravat *et al.* 1995) is longer than a wavelength of 600 km. The regional-scale magnetic anomalies derived from Magsat data (e.g. von Frese *et al.* 1982; Nakatsuka & Ono 1984) have a resolution longer than a wavelength of 400 km. The logarithm of energy versus wavenumber (Fig. 3) shows that the energy of wavenumbers higher than 29 is four orders of magnitude smaller than the energy of wavenumber 5, implying that the amplitude of the magnetic anomalies produced by all of these higher wavenumbers is about two orders of magnitude less than that produced by the lower wavenumbers. The anomalies

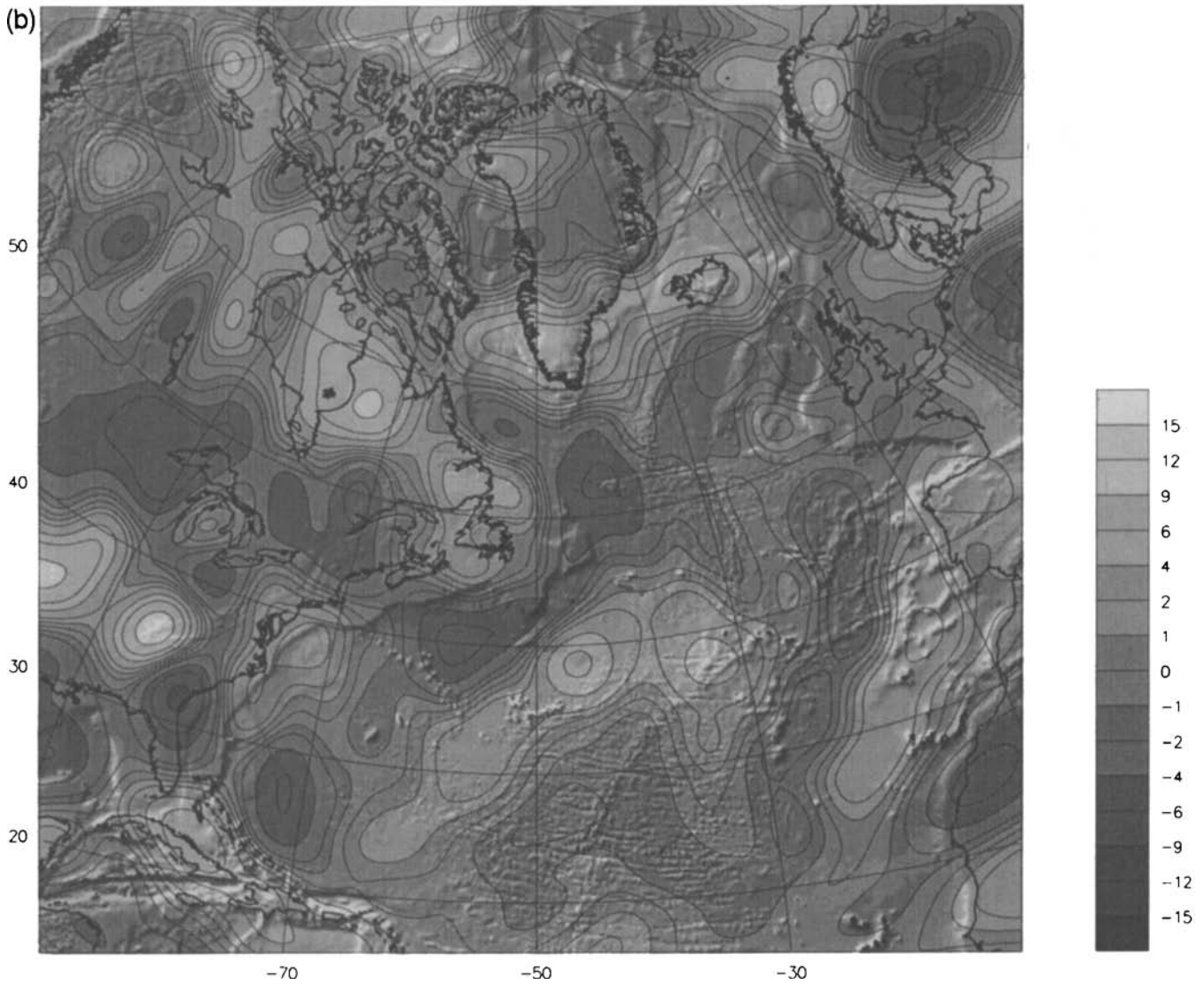

Figure 2. (*Continued.*)

seen in the North Atlantic maps span an amplitude range from -15 to $+15$ nT, suggesting that less than 0.15 nT is contributed by these high wavenumbers; this is substantially less than the 2 nT error limit of the maps. We investigated this point by calculating magnetic anomalies from the three data sets using K values greater than 29. These anomalies had amplitudes of less than ± 0.2 nT. The Magsat anomalies were strongly dominated by elongated features which were parallel to the satellite tracks, similar to those seen by other investigators elsewhere (e.g. Arkani-Hamed & Strangway 1986). The POGO anomalies were more or less equidimensional, probably produced by the interference of elongated features parallel to the tracks of the POGO satellites, the interference arising from the crossings of the tracks. Wavenumbers higher than 65 (wavelengths shorter than 157 km) have an almost white noise behaviour with energies over three orders of magnitude less than wavenumber 29. They are most likely dominated by data-processing errors and non-lithospheric sources. These characteristics of the energy spectra suggest an appropriate bandpass filter in order to extract those anomalies which are most likely of lithospheric origin. The filter we use is circular in the 2-D Fourier domain. It removes all harmonics with K values smaller than 3 and greater than 35, and leaves unchanged those harmonics with K values between 5 and 29. The harmonics with K values between 3 and 5, and 29 and 35 are suppressed through multiplication with Hanning functions.

The three magnetic anomaly maps, POGO, dawn and dusk, provide a unique opportunity to derive a satellite magnetic anomaly map of the North Atlantic Ocean based on their common features, and to assess the error limits of the anomalies using their standard deviations. These common features are selected by covariance analysis. Fig. 4(a) shows the degree correlation coefficients, μ_k, of these three maps calculated using the method adopted by Arkani-Hamed & Strangway (1986),

$$\mu_k = \frac{\text{Real}\left[\sum_{uv}\left(F_{u,v}G^*_{u,v} + F_{u,-v}G^*_{u,-v}\right)\right]}{\left[\sum_{uv}\left(|F_{u,v}|^2 + |F_{u,-v}|^2\right).\sum_{uv}\left(|G_{u,v}|^2 + G_{u,-v}|^2\right)\right]^{1/2}}. \quad (4)$$

The degree correlation coefficients decrease from $K=5$ to $K=20$ and then increase up to $K=25$, beyond which they increase

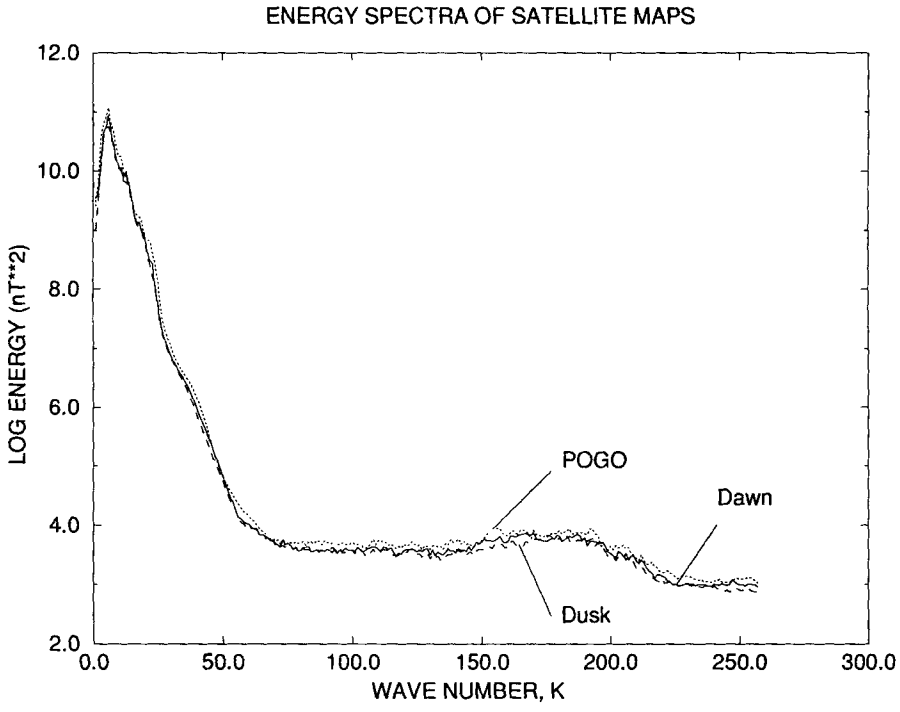

Figure 3. The energy spectra of POGO, dawn and dusk maps of the North Atlantic Ocean.

slowly. The minimum correlation around the K value of 20 is typical for all three degree correlation curves, and is probably due to the remaining external magnetic field effects. The northern parts of the maps underlie the auroral zone with a strong external magnetic field, which was probably not removed completely by the along-track cleaning conducted by Ravat *et al.* (1995).

Arkani-Hamed & Strangway (1986) used a covariance technique to extract common features of Magsat dawn and dusk maps of the Middle East and Eastern Europe. Following their procedure, we made many experiments with the cut-off values of the signal-to-noise ratio. As the cut-off value increased, the correlation of the selected covariant harmonics improved while the retained power decreased. The signal-to-noise ratio greater than or equal to 1.5 made good improvement on the degree correlation coefficients and yet retained over 50 per cent of the original power; this is the value adopted in this study. Fig. 4(b) shows the degree correlation coefficients obtained using these covariant harmonics. The selection criterion has significantly enhanced the degree correlations: the correlation coefficients are now above 0.5 and typically above 0.6. Note that the improvement is very drastic for the wavenumbers around 20.

The application of the covariance criterion and the bandpass filter to the three satellite maps led to six sets of bandpass-filtered maps, POGO–dawn, dawn–POGO, POGO–dusk, dusk–POGO, dawn–dusk and dusk–dawn. POGO–dawn denotes the covariant part of the POGO map retained when comparing POGO and dawn maps, and dawn–POGO denotes the covariant part of the dawn map retained when comparing the POGO and dawn maps, and so on. These six maps were combined into a final bandpass-filtered satellite magnetic anomaly map of the North Atlantic Ocean (Fig. 5a) by simple averaging. Fig. 5(b) shows the standard deviation of the anomalies seen in Fig. 5(a), calculated by

$$\sigma = \left[\sum_{i=1}^{6} (B_f - B_i)^2/6 \right]^{1/2}, \qquad (5)$$

where B_i, $i = 1,\ldots,6$, denotes the magnetic anomaly at a given location of the ith map, and B_f is the averaged magnetic anomaly at that location. The standard deviations are less than 2 nT, except in a few localities that are not situated over the North Atlantic Ocean. A comparison of Figs 5(a) and (b) shows that the prominent magnetic anomalies of the North Atlantic Ocean have very small standard deviations, and thus are reliable.

THE MARINE MAGNETIC ANOMALY MAP OF THE NORTH ATLANTIC OCEAN

We use a new data base of shipborne magnetic measurements to derive the intermediate-wavelength marine magnetic anomaly map of the North Atlantic Ocean. This data base was constructed as part of a major compilation of all the magnetic data in the North Atlantic and Arctic oceans and their surrounding land masses (Verhoef *et al.* 1994). In the following paragraphs we discuss major steps in the removal of non-lithospheric components from the magnetic observations and present the resulting marine magnetic anomaly map.

The shipborne magnetic data base consists of 656 cruises from the period 1956–92, representing about 6.5 million data points and 3 million line kilometres. About 55 per cent of the data were collected in the 1970s, about 20 per cent prior to 1970 and about 25 per cent after 1980. It is compiled from original observations that have been obtained directly from many different organizations, or indirectly from the National Geophysical Data Center in Boulder, Colorado. The navigation ranged from celestial navigation to Global Positioning

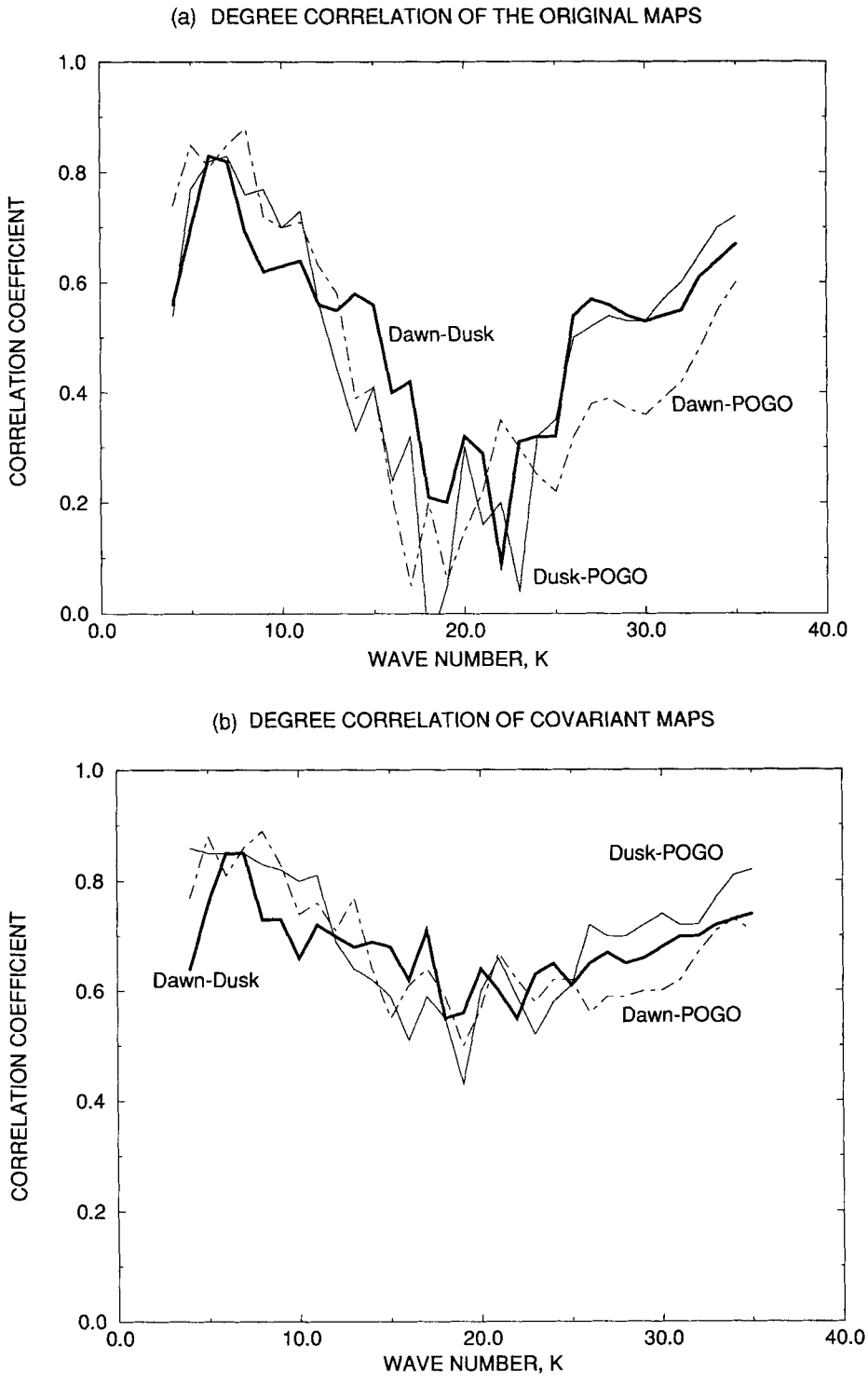

Figure 4. Degree correlation coefficients between the satellite maps of the North Atlantic Ocean. (a) The coefficients computed using all the harmonics and (b) the coefficients calculated using the covariant harmonics with signal-to-noise ratios larger than or equal to 1.5.

System navigation, therefore the quality of the data is highly variable, the older data being less accurate. Prior to a statistical analysis of the data, spikes and other obviously erroneous data points are identified and corrected, using generalized forms of the fourth-order difference method (Hood, Holroyd & McGrath 1979) and the Naudy filter (Naudy & Dryer 1968). The generalization takes into account the variable sampling intervals. Despiking is carried out iteratively; the data point with the highest fourth-order value is corrected at each iteration until there is no fourth-order value left that exceeds the threshold. The threshold level for detecting faulty data depends on parameters such as the depth of the magnetic sources, and

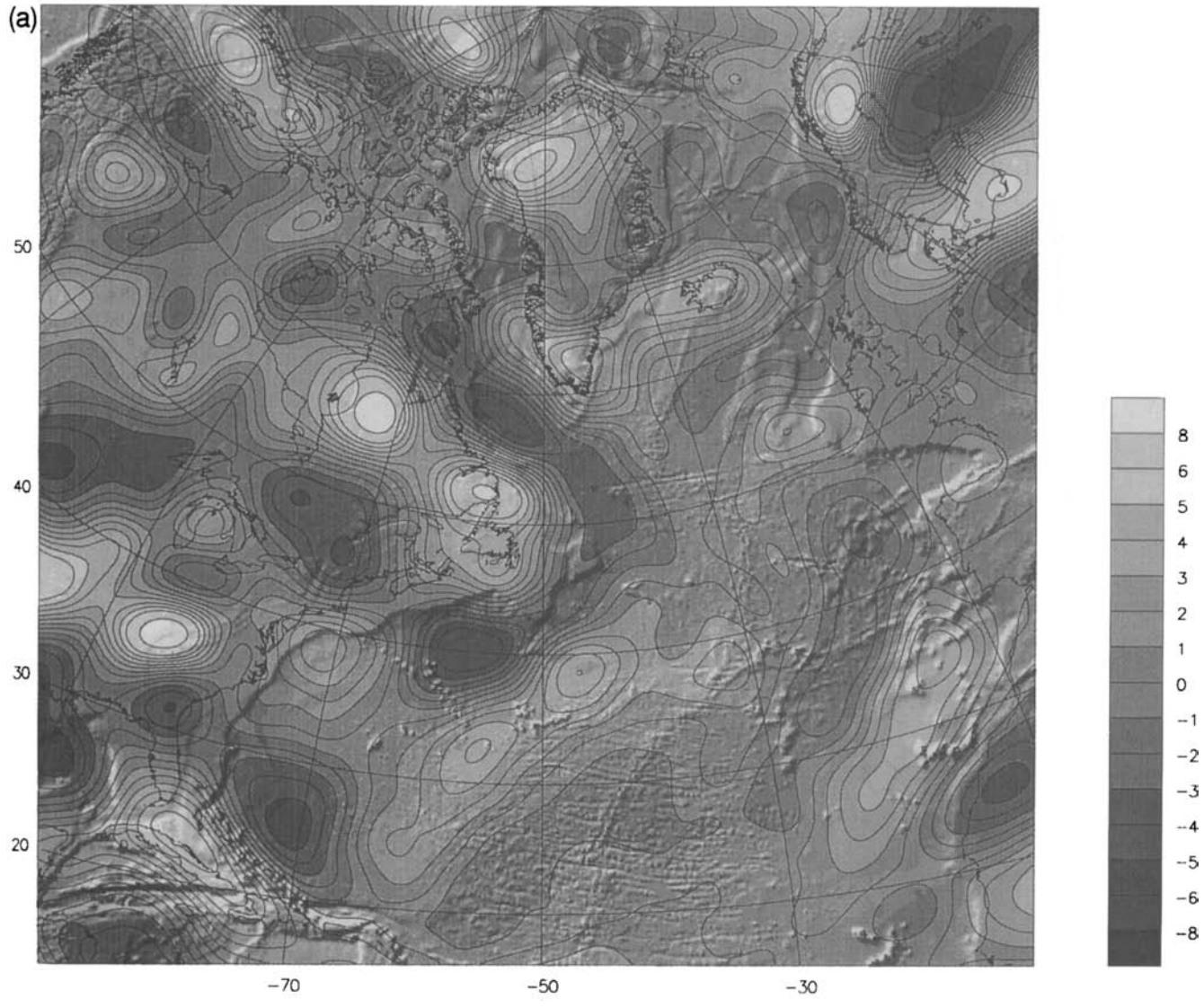

Figure 5. (a) Combined satellite magnetic anomaly map of the North Atlantic Ocean, and (b) the standard deviations of the anomalies. Note that the contour interval for the standard deviation is 0.5 nT.

the sampling intervals. We determined the threshold using two synthetic profiles of high derivative values, one over a point source and another over a magnetic contrast located at varying depths. The algorithm was also tested with actual observations from Davis Strait, which cover both deep ocean and shallow waters. In addition, we visually scanned all data and corrected or removed data where required.

Cross-over analysis

We assess the quality of the data and the effectiveness of the various processing steps with a statistical analysis of the cross-over errors, which are observational discrepancies at the intersections of ship tracks, and which are due to non-lithospheric sources. There are 148 227 cross-overs in the data base. The standard deviation of the errors is about 93 nT. Cross-over errors in cruises prior to 1965 are significantly larger than those of the recent ones, probably on account of navigational inaccuracy of the older cruises.

The various types of errors that affect the marine magnetic measurements are divided into two major groups: operational errors, arising from undetectable level changes in the short segments of the data and from the magnetic effect of the ship; and non-lithospheric magnetic fields effects, arising from the external magnetic field contributions and the inaccuracy of the core-field models that are used to remove the core-field contribution to the measurements.

Operational errors

Shipborne data are usually collected continuously and any sudden jump in the level of the data can be easily detected. However, in cases when the data contain many short segments it is difficult to detect possible level shifts. The data base is checked for 'isolated' segments, detected when the length of the segment is less than 10 km and the gaps on either side are longer than 5 km. Numerous isolated segments are found and removed. In particular, the data collected prior to 1965 have relatively more isolated segments: only 1.8 per cent of the data base was collected prior to 1965, but that part of the data base

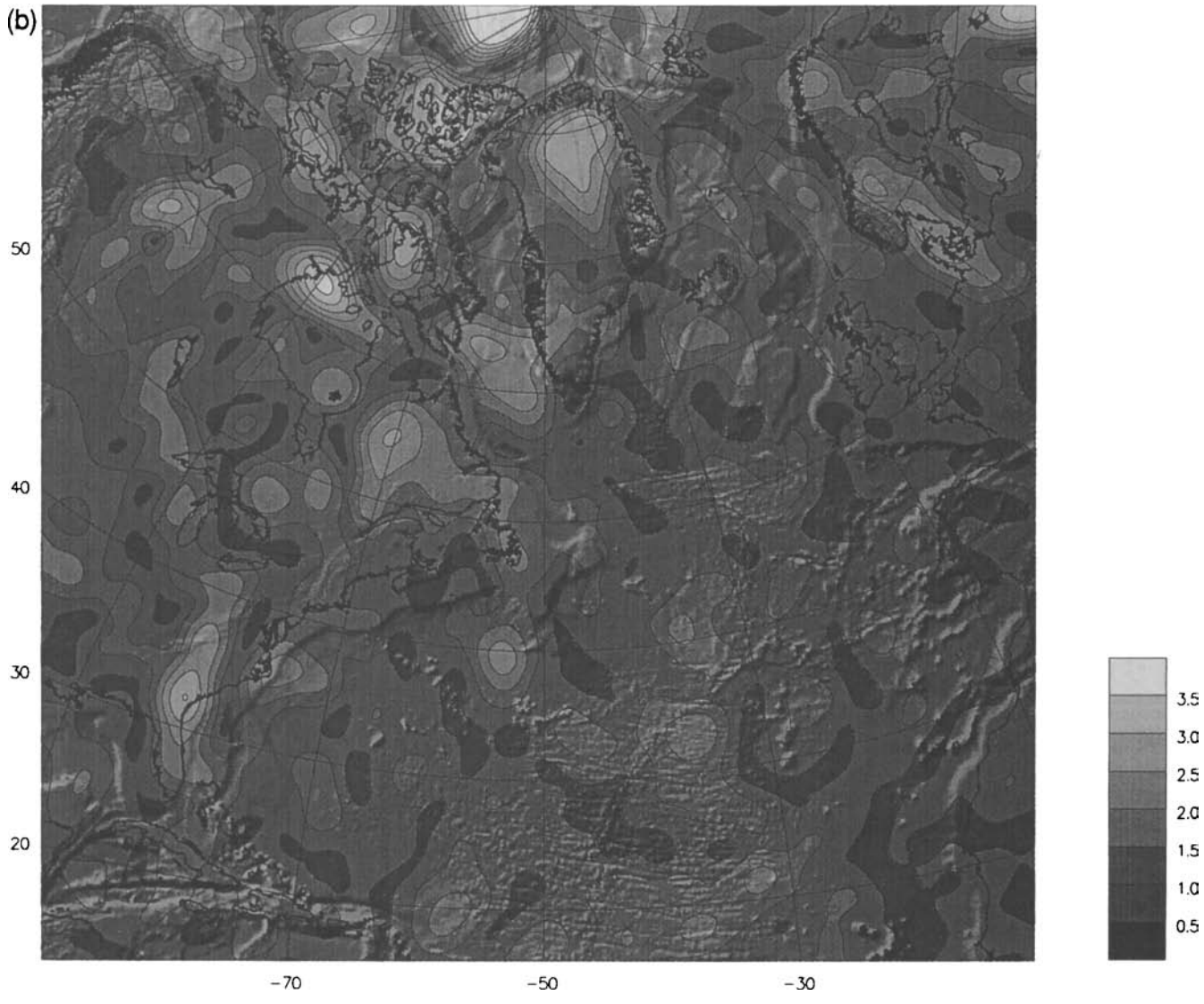

Figure 5. (*Continued.*)

contains about 26 per cent of the isolated segments. Therefore, we eliminate the data collected prior to 1965, because of their large cross-over errors and sampling distances, and because they are located in areas where there is more recent coverage.

We also examine the magnetic effect of the ship (Bullard & Mason 1961). The effect is calculated using the cross-overs of those cruises each having more than 50 internal crossings, i.e. the crossings of an individual survey with itself (crossing tracks with an angle less than 20° are not used because a small navigation error might shift the location of the cross point substantially). This is the case for about 100 cruises in our data base and the rms of the ship effect is found to be about 5 nT, not important for most of the cruises. Therefore, the magnetic data base is not corrected for the magnetic effects of the ships.

Non-lithospheric magnetic field effects

To assess the effects of the external magnetic field on the cross-over errors we investigate the possible relationship between the errors and the Kp and AE indices as well as the diurnal variations of the field. The planetary activity index Kp is based upon the magnetic field variations measured at geomagnetic observatories and tabulated at one value per three hours, ranging from 0, very quiet, to 9, very disturbed (Lincoln 1967). The auroral electrojet (AE) index indicates the difference between the eastward and westward electrojet and a high value denotes a high auroral electrojet activity. The index is tabulated at one value per hour (e.g. Mayhaud 1980). The Kp indices are available from 1955 on, and AE values are available from 1965 until 1987, with the exception of 1976 and 1977. These indices are also used for the selection of the quiet magnetic field satellite data. The area is divided into two regions, the southern region south of 60°N, and the northern one north of 60°N. The Kp index is used for the southern region and the AE index for the northern, except during 1976–77 and after 1987, when the Kp index is used in the absence of the AE index. A plot of the AE versus the Kp indices shows that high Kp values correspond to high AE values, although with a large scatter, which qualitatively justifies our substitution.

The distribution of the number of observations versus time and the number of cross-overs versus time are very similar,

suggesting that the cross-over data are representative of the entire data base. We examine the cross-over errors for different Kp or AE values on the premise that the improvement of the cross-over statistics resulting from the removal of data acquired during high Kp or AE values provides a good estimate for the improvement of the entire data base. The cross-over errors significantly increase when we include the measurements which are acquired when the Kp index is larger than 5. For the AE index, the cut-off value is found to be about 600. Therefore, we eliminate all the cross-overs when at least one of the intersecting tracks occurs during the time when the Kp index exceeds 5, or the AE index is larger than 600. This elimination decreases the standard deviation of the cross-over errors by about 3.5 nT (about 4 per cent).

We next consider the effects of the magnetic disturbances caused by the perturbations of the ring-current and the associated induced current inside the Earth. The magnetic data base is corrected for these effects using the time and latitudes of the observations and adopting the simplified expression by LaBrecque, Cande & Jarrard (1985). The corrections are generally small; their averages range from about -8 nT in the southern part to about $+2$ nT in the north.

Magnetic observations should be corrected for the diurnal variations of the geomagnetic field arising from the dynamo current in the ionosphere during the data acquisition, usually by subtracting the time variations detected at a nearby magnetic observatory. As a rule, shipborne magnetic data are not corrected for the diurnal variations, mainly because of the large distances between a land observatory and the survey areas and differences in the diurnal characteristics of coastal regions and oceans due to induced current (Rikitake 1966). LaBrecque *et al.* (1985) used Malin's (1973) global model of the diurnal variations to correct their shipborne data in the North Pacific. We use our magnetic data base to extract a diurnal signal by removing effects of geological features through stacking the data as a function of the local time in geomagnetic latitude bands (the diurnal variations as a function of latitude are best described in the geomagnetic coordinate system). The geological effects are removed by averaging all cross-over errors in latitude bands of 10° and in bins of

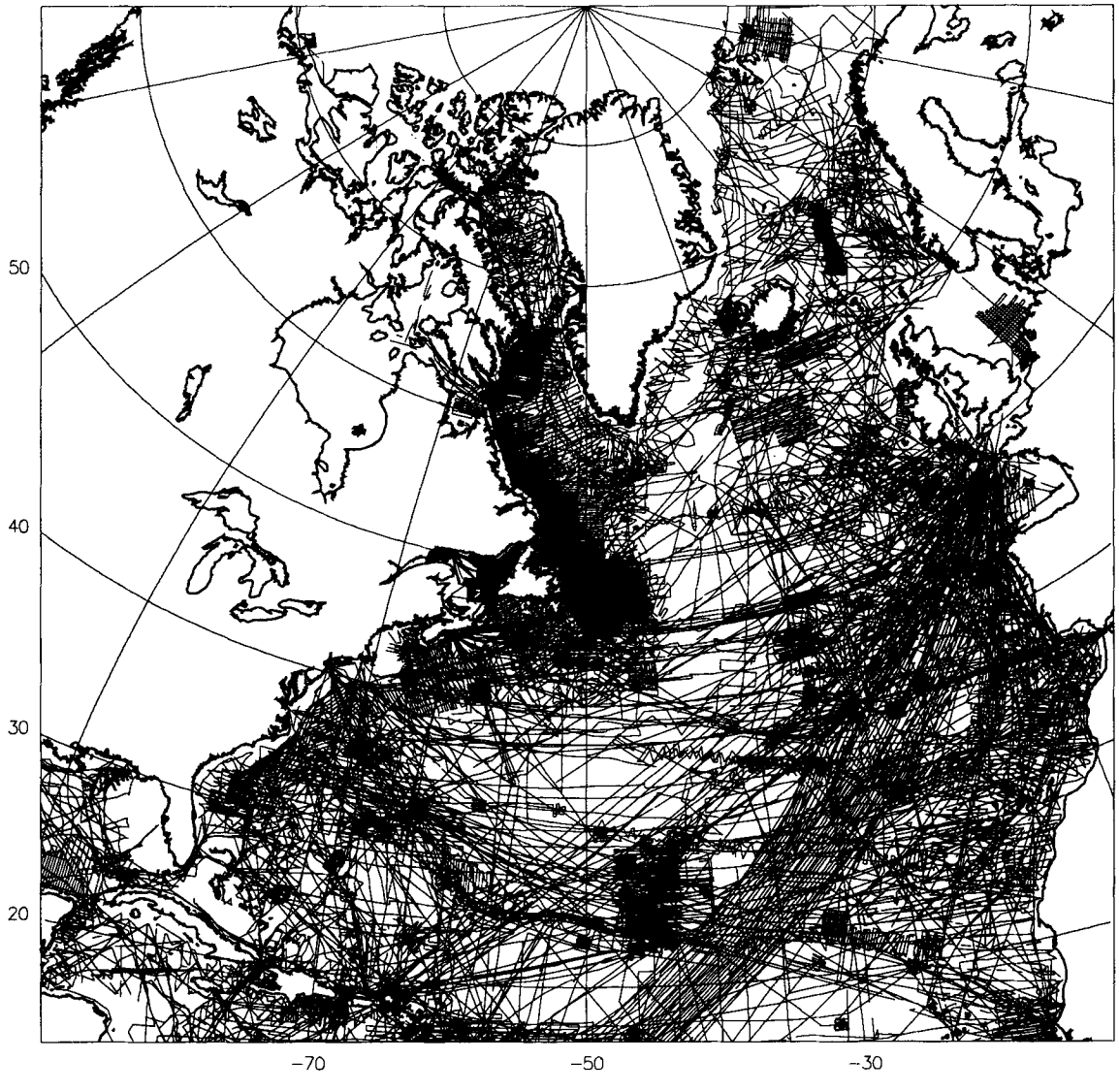

Figure 6. The distribution of ship tracks, after removal of erroneous data.

1 hour local time. Cross-over data are better suited for removing the geological effects because the data are not biased by particular geological features of high-amplitude anomalies, like the oceanic ridges and fracture zones. Our diurnal variations differ from that predicted by Malin's model, to a small extent in low latitudes but significantly in latitudes higher than about 50°. The reason for these discrepancies is unclear, but it may be related to the distribution of the land-based observatories used in Malin's (1973) model, which is based on quiet day variations for the interval of 1957–60 at 100 geomagnetic observatories with a relatively high number located in Europe. The diurnal variation measurements of the observatory at the Atlantic Geoscience Centre (located at approximately 45°N) compare favourably with our calculations in the latitude band of 40–50°N. Also, there is good agreement between our diurnal variations and those of a moored magnetometer on Baffin Bay at about 70° latitude (Jackson *et al.* 1979), implying that our model probably better describes the diurnal variations in this part of the world. Consequently, our regional model was adopted to correct the diurnal variations in the data, thereby reducing the standard deviation of the cross-over errors by 2.1 nT (about 3 per cent).

The above processes reduce the standard deviation of the cross-over errors from about 93 nT to about 75 nT, an improvement of about 20 per cent. Accordingly, these cleaning processes are adopted for the entire data base. After the corrections, some segments are identified as being abnormal (by a preliminary gridding of the entire data) and are deleted. In total about 500 000 data points are deleted by all the above processes and the cleaned data base contains a total of about 6 000 000 data points. Fig. 6 shows the track lines of these selected data. The data coverage is very dense in the continental margins, but becomes less dense in the middle of the ocean, especially in the southern parts.

Another potential source of error is the geomagnetic reference field models. The shipborne data are reduced to magnetic anomalies by removing the core-field contribution as modelled by the appropriate IGRF. Since the data base spans a period of about 27 years, the corrections for the secular variations of the core field become important. Although the IGRF models take these variations into account, an earlier cross-over analysis of the data in the western North Atlantic (Verhoef & Macnab 1989) suggests that the IGRF models may not accurately represent the temporal core-field variations over the North Atlantic Ocean. The application of the IGRF models may have removed parts of the broad-scale lithospheric field together with the core field, or it may not have removed the entire core-field contribution. Fig. 7 shows the low-pass-filtered marine magnetic anomalies of the North Atlantic Ocean. The filter is applied in the space domain using a 2-D Hanning bell with a radius of 400 km. There is a pronounced broad anomaly almost parallel to the geomagnetic latitudes with an amplitude which is decreasing northward. This anomaly covers many different geological features and partly overlaps the core field, suggesting that it is substantially contaminated by the removal of the IGRF models. Therefore, similar to the satellite magnetic anomalies, the long-wavelength components of the marine magnetic anomalies may not be reliable.

Marine magnetic anomaly map

To derive an intermediate-wavelength marine magnetic anomaly map of the North Atlantic Ocean the cleaned marine data are first gridded at 20 km intervals, using the same projection and areal coverage as the satellite maps. The grid values in the oceanic areas are determined through weighted averaging of the neighbouring data using a 2-D Hanning bell in the space domain with a diameter of 400 km as a weighting function. The grid values on the continents are set to zero, except within a narrow shoreline band of 200 km where the marine data are extended outside the data coverage onto the continents and then tapered to zero. The gridded data are Fourier analysed and bandpass filtered using the same filter applied to the satellite anomalies. Fig. 8(a) shows the resulting bandpass-filtered marine magnetic anomaly map of the North Atlantic Ocean at sea level. Comparison with Fig. 7 shows that the large regional trend that overlaps with the core field has largely been removed, especially in the southern parts. The geophysical implications of these anomalies will be discussed in the next section.

For a direct comparison with the satellite observations, the marine magnetic map was upward continued to 400 km altitude using the Fourier domain algorithm (Fig. 8b). Comparison of Figs 8(a) and (b) shows that the upward continuation has minor effects on the long-wavelength features but substantially reduces the amplitudes of the short-wavelength ones. Small features, such as the positive anomaly in the south of the Rockall Plateau and the negative anomaly in the north-east of the Nova Scotia Basin are diminished through the upward continuation. Some small but nearby anomalies of similar sign, such as the two positive anomalies, one to the north and the other to the south of Newfoundland, and the two negative anomalies in the Labrador Sea, are merged producing broader anomalies at the satellite altitude.

DISCUSSION AND CONCLUSIONS

Figs 5(a) and 8(b) present two intermediate-wavelength scalar magnetic anomaly maps of the North Atlantic Ocean at 400 km altitude, derived from two completely independent data sets which were acquired at two very different altitudes and times using different magnetometers. Except for the final stage of extracting the intermediate-wavelength components from the satellite and shipborne data by bandpass filtering, the data processing used for the cleaning and derivation of the final maps is also independent. It is therefore reasonable to assume that their common features most likely arise from lithospheric sources. There are many differences between the two maps over small-scale and low-amplitude features, particularly over the shorelines where anomalies are tapered to zero within the shoreline band of 200 km described above, as seen in Fig. 9 which shows the difference between the satellite anomalies and the upward continued marine magnetic anomalies. These arise from the fact that the satellite map contains data from the continents as well as the ocean, whereas the marine map is derived from the oceanic measurements alone. For example, the marine map has a significantly weaker amplitude over the Iceland–Faroe ridge compared to the satellite map, because the high-amplitude magnetic data onshore, which are a part of the satellite data, are not included in the marine data set. Similar uncertainties are related to the positive anomalies north and south of Newfoundland (Fig. 8a). The upward continuation has merged these anomalies, resulting in a broader anomaly with a maximum directly overlying Newfoundland, whereas the corresponding anomaly

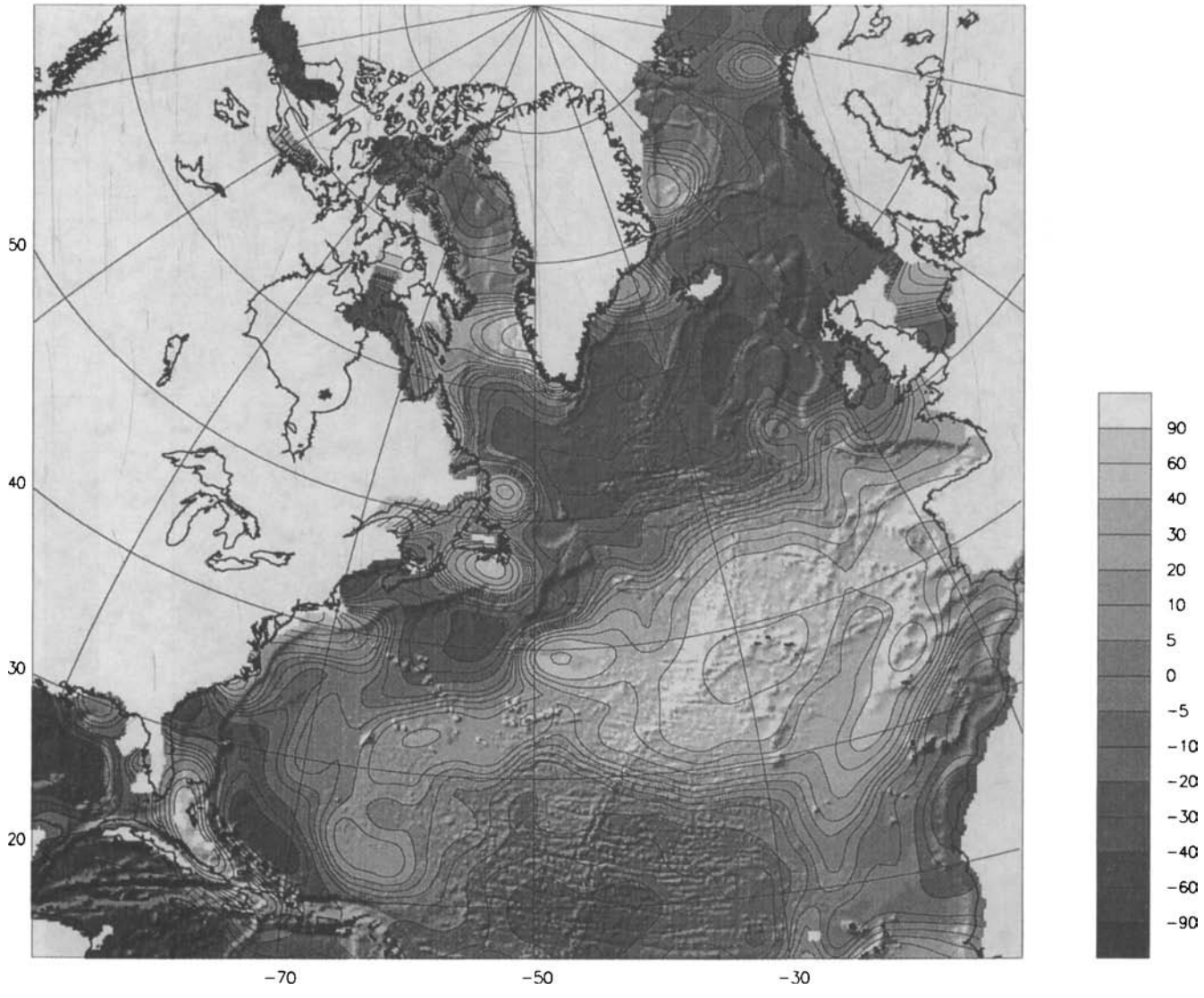

Figure 7. Low-pass-filtered marine magnetic anomalies of the North Atlantic Ocean. A Hanning bell function with a radius of 400 km was applied in the space domain to remove the shorter wavelengths.

in the POGO and Magsat maps (Figs 1 and 2) is located in the north with an elongated peak largely overlying the continental area, although the satellite maps have discrepancies about the amplitude of the anomaly. The positive anomaly in the marine map off the north-east of Greenland does not exist in the combined satellite map and in the original POGO and Magsat maps (Figs 1, 2a and 2b), nor does it exist in the scalar magnetic anomaly map of the north pole derived from Magsat data by Coles (1985). The anomaly is located close to the north geomagnetic pole where the magnetic anomaly and the ΔZ component of the magnetic field of a body are expected to be almost identical. Nevertheless, the ΔZ anomaly map of the north polar region by Haines (1985), and those recently derived from Magsat vector data by Ravat *et al.* (1995) do not show a positive anomaly in this region either. The existing aeromagnetic profiles over this region show a positive magnetic anomaly but with a relatively smaller size and lower amplitude. It is worth noting that the density of the ship tracks in this region is quite low (Fig. 6) so the surface anomaly is produced by interpolation of relatively sparse data, the process which has probably broadened the anomaly. The actual size of the anomaly is probably small and its amplitude at satellite altitudes is lower than the noise level of satellite data. Therefore the high amplitude shown for this anomaly on the upward continued marine map may not be reliable.

The marine and satellite maps contain similar but not identical harmonics. The covariance selection criterion has removed several harmonics from the satellite map which were not common among the POGO and Magsat maps: they were contaminated by non-lithospheric sources. The northern part of the study region lies below the auroral oval and the auroral electrojets may have significantly contributed to those rejected harmonics. The contribution to the retained harmonics of the satellite map (Fig. 5a) is most likely minor due to the stringent covariance selection criterion adopted. Although the marine data are corrected for the external magnetic field effects, no selection criterion is used to remove some of the harmonics, expect for the bandpass filter. It is possible that the auroral effects have contaminated some of the features of the marine map with wavelengths comparable to the lithospheric magnetic anomalies.

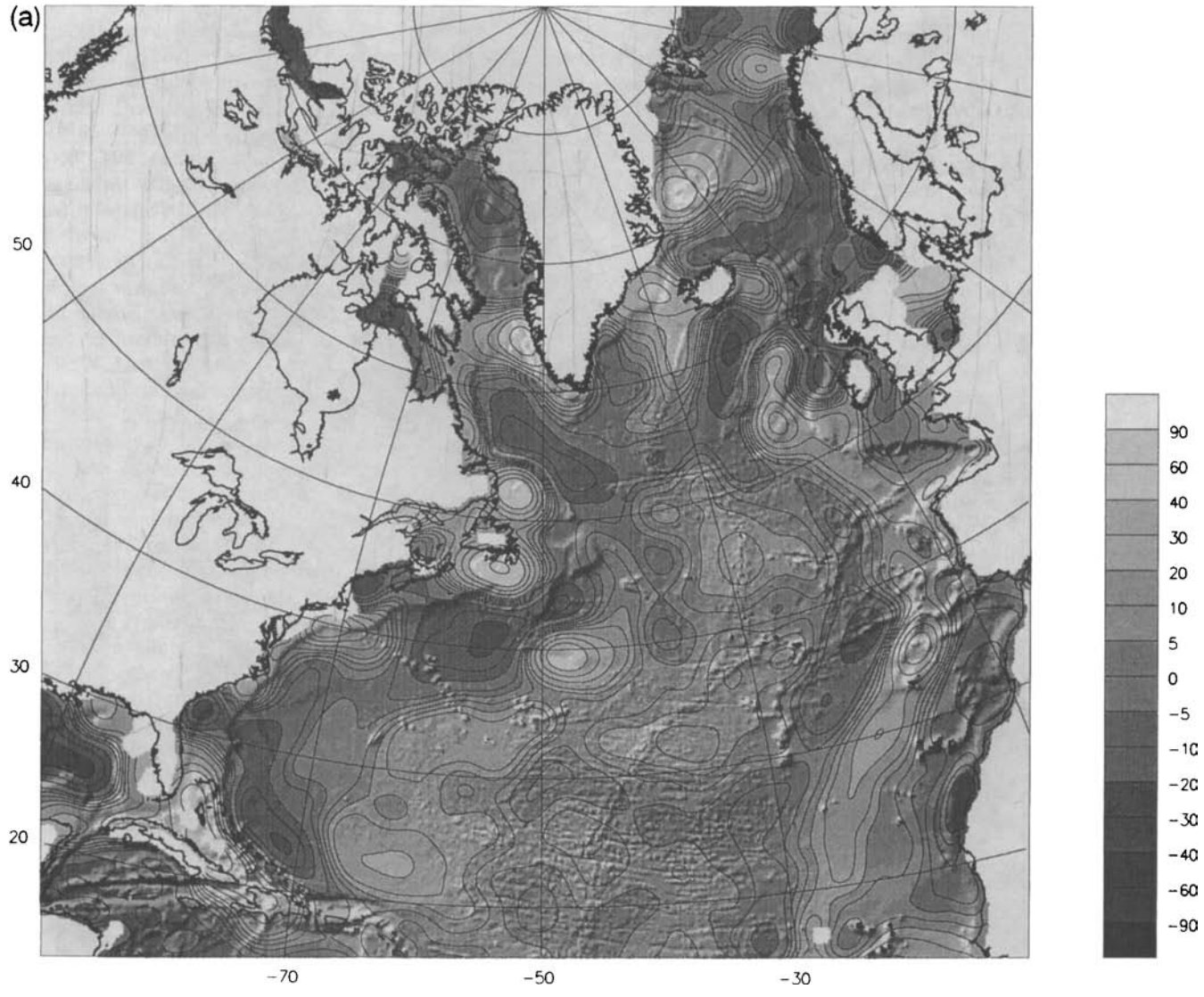

Figure 8. Intermediate-wavelength, bandpass-filtered, marine magnetic anomaly map of the North Atlantic Ocean (a) at sea level, and (b) upward continued to 400 km altitude.

In spite of the above differences, there is excellent agreement between the more prominent marine and satellite magnetic anomalies. The well-defined and high-amplitude anomalies of both maps are almost identical in amplitude and location. In general, the discrepancies between well-defined anomalies are much smaller than the amplitude of the anomalies in the two original data sets. No appreciable residual is shown on Fig. 9 for the large negative anomalies in the Labrador Sea, Nova Scotia Basin and north-east of Cuba, and the positive anomalies associated with the Cretaceous quiet zones (CQZ). A large discrepancy occurs in the north. Because of the relatively narrow widths of the Labrador and Norwegian–Greenland seas and the fact that data over continents are set to zero, the broad anomalies in the marine map are truncated and reduced to intermediate-wavelength anomalies. Consequently, the bandpass filter has not removed them effectively, as seen comparing the energy spectra of the satellite and the upward continued marine anomalies (Fig. 10). Other differences are mainly near the ocean–continent boundary and probably arise from the edge effects and tapering the marine data within the shoreline band. LaBrecque & Cande (1984) compared the bandpass filtered and upward continued marine magnetic anomaly map over the Central Pacific with the Magsat map available at that time, and concluded that the amplitude of the marine anomalies was about a factor of 2 greater than that of Magsat anomalies. They related this discrepancy to the Magsat data processing for removing the external field components. The large discrepancy in their results is most likely due to the relatively subdued nature of the short-wavelength components of the old Magsat map they used (see their Figs 5 and 6) compared to their marine map. The short wavelengths of the satellite map we use in this paper have relatively greater amplitudes.

Fig. 10 shows the energy spectra of the satellite magnetic anomalies and the upward continued marine anomalies for comparison. Fig. 5(a) contains both oceanic and continental areas, whereas Fig. 8(b) is based on only the marine data. To produce a comparable energy spectrum, the satellite map is masked using the marine map by setting the anomalies over the continents to zero, and tapering the shoreline band to zero

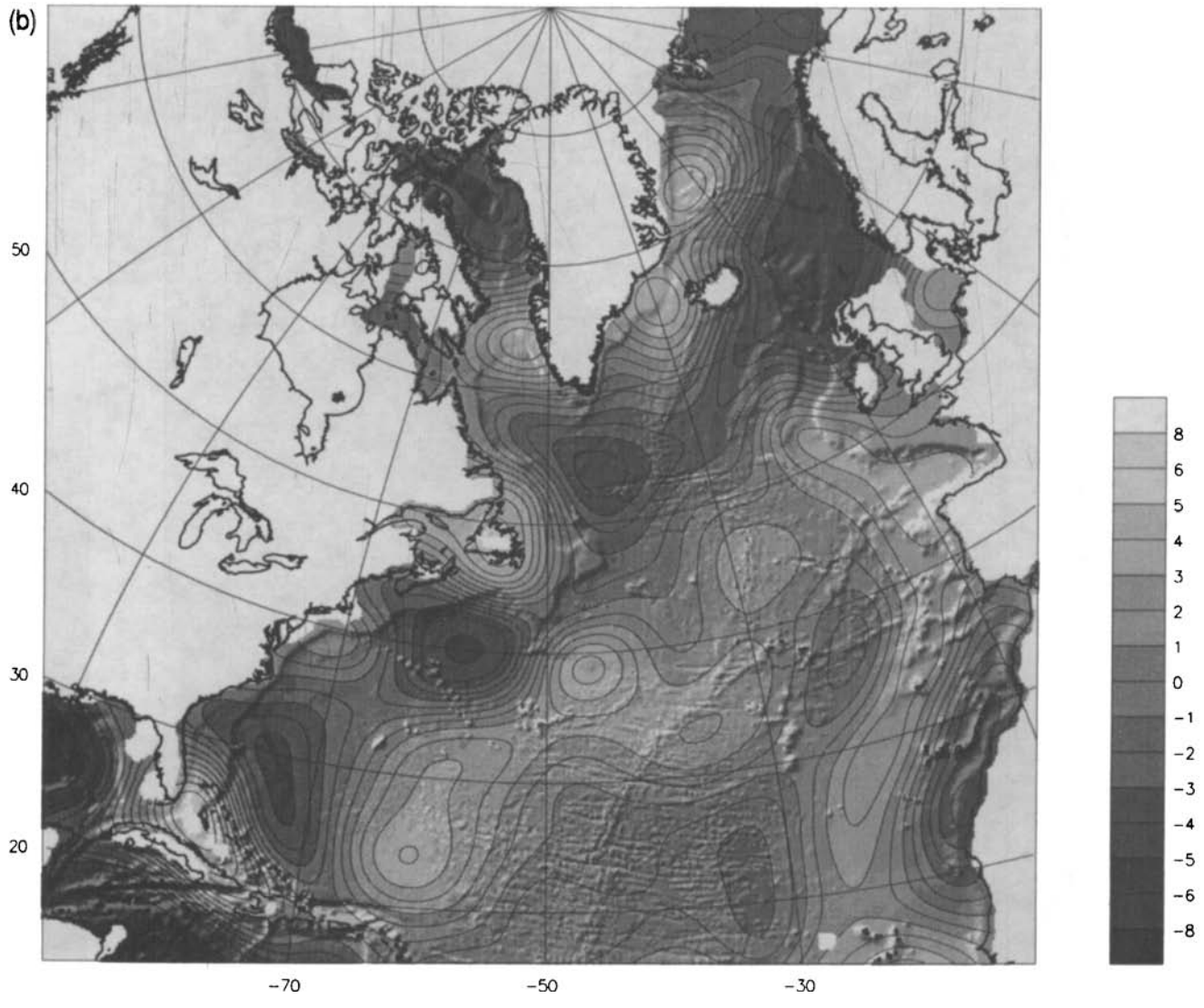

Figure 8. (*Continued.*)

as done for the marine map. The close similarity of the energy spectra of the upward continued marine map and the masked satellite map further emphasizes that the intermediate-wavelength magnetic anomalies derived from satellite and marine data are real and that they reflect the lateral variations in the magnetization of the lithosphere of the North Atlantic Ocean.

The comparison of Figs 8(a) and (b) shows that several apparently intermediate–wavelength anomalies at the satellite altitude arise from a combination of small neighbouring features of the sea level map as mentioned before. The anomalies must be interpreted in terms of these small features, rather than some fictitious large-scale sources. However, many well-defined anomalies seen on both satellite and marine maps are associated with known broad-scale geological features. Here we discuss the geophysical significance of these large-scale anomalies and the constraints they impose on the magnetization of the oceanic lithosphere. In relating the magnetic anomalies to geological features it should be noted that the anomalies are not reduced to the pole. This has little effect on the anomalies in the north where the core field is almost vertical. In the south, anomalies are shifted towards the equator with respect to their source bodies, but by not more than 300 km, which is short compared with the sizes of the pronounced anomalies in this region.

Most seafloor-spreading magnetic anomalies reduce below the noise level at satellite altitudes due to strong attenuation of the amplitude of high-frequency signal. The CQZ of oceanic areas are, however, formed during a long period (about 30 Myr) of normal polarity and they produce well-defined magnetic anomalies at satellite altitudes (e.g. LaBrecque & Raymond 1985; Fullerton *et al.* 1989; Toft & Arkani-Hamed 1992). A comparison of Figs 5(a) and 8(b) shows that the shipborne observations over the CQZs of the North Atlantic (see Fig. 11 for the locations cited in this paper) are in excellent agreement with the satellite data, as was also demonstrated by LaBrecque & Raymond (1985). It is worth noting that the positive CQZ anomalies in Figs 5(a) and 8(b) are not centred directly over the CQZ due to the large anomalous skewness of the anomalies and the fact that they are not reduced to the geomagnetic pole. Modelling these anomalies in terms of the NRM of the oceanic layer 2A (LaBrecque & Raymond 1985)

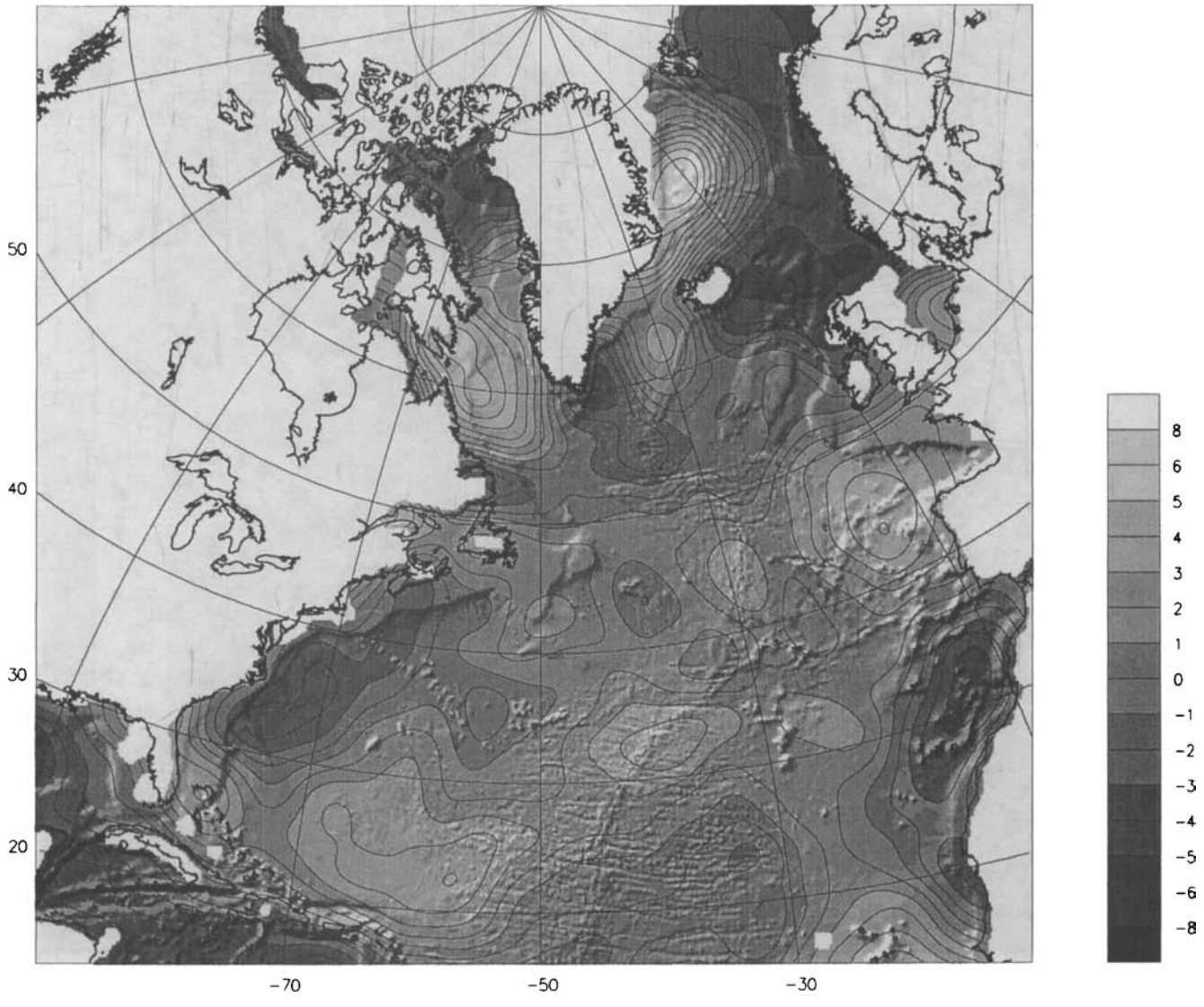

Figure 9. Difference between the upward continued marine magnetic anomalies and satellite anomalies (Fig. 8b minus Fig. 5a).

requires about twice more magnetization than that of a normal 80 million year old layer 2A (Bleil & Petersen 1983), suggesting significant contributions from deeper sources.

The Labrador Sea is another area where the seafloor-spreading anomalies yield a significant negative anomaly at satellite altitude, due to the dominantly reversed polarity during a 50–65 Ma period (Arkani-Hamed 1990). Bradley & Frey (1991) related this anomaly to the possibility that a weakly magnetic Labrador Sea lithosphere is sandwiched between two highly magnetic continental lithospheres of Greenland and eastern Canada, and the anomaly is produced due to the uncertainty of the zero level in the data processing. This interpretation, however, is not supported by our marine magnetic anomaly map (Fig. 8b). As mentioned earlier, the marine map has no contribution from the continental data. Nevertheless, the Labrador Sea is delineated by a negative marine magnetic anomaly with good correlation to that seen on the satellite map (Fig. 5a), indicated by a negligible difference in Fig. 9. This suggests that a significant portion of the anomaly probably arises from the contribution of the seafloor-spreading anomalies.

A puzzling result of satellite magnetic observations is the lack of a consistent magnetic anomaly associated with the ocean–continent passive margins where two chemically and physically different lithospheres are juxtaposed. An upper limit of 37 000 A is estimated for the bulk (vertically integrated) ocean–continent magnetization contrast across the east coast of North America (Arkani-Hamed 1993), which is in good agreement with the contrast of 33 000 A found by Counil, Cohen & Achache (1991) on a global scale. Many factors may contribute to the magnetic character of the margins, including the amount of volcanism during continental rifting; the polarity of the core field during rifting and subsequent episode of seafloor spreading; and the sedimentary cover. All have effects on the short-wavelength magnetic signature of the margins. Going from south to north in the North Atlantic, the continental breakup becomes progressively younger, with individual sections of the margin breaking up during times of normal and reversed core-field polarity. In addition, parts of the margin, in particular in the Norwegian–Greenland Sea, are characterized by intensive volcanic activities (White & McKenzie 1989; Eldholm & Grue 1994). However, except for

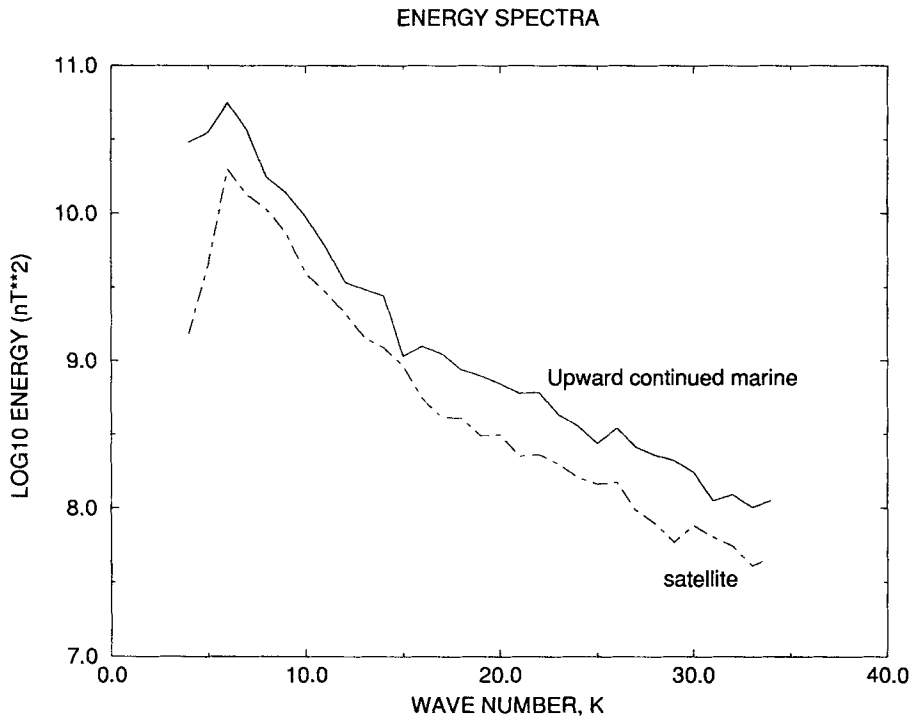

Figure 10. The energy spectra of the satellite and upward continued marine magnetic anomaly maps of the North Atlantic Ocean at 400 km altitude.

the south-west Greenland margin which has a positive anomaly at satellite altitudes, there is no consistent intermediate-wavelength magnetic signature associated with the margin. In contrast, the deep marginal basin of Nova Scotia has a well-defined negative satellite anomaly, as also shown on the global maps over this basin and other deep marginal basins such as the Bay of Bengal, and the Australian Bight (e.g. Arkani-Hamed *et al.* 1994). Detailed studies of the thermal evolution of the oceanic lithosphere beneath the Nova Scotia Basin (Ghods 1994) indicate that thermal demagnetization of the oceanic crust due to thermal blanketing effects of the sedimentary layer is not significant, as the sedimentary cover of the oceanic lithosphere in this basin is only about 4 km thick. The source of the pronounced negative anomaly of the basin is still poorly understood.

The intermediate-wavelength anomalies clearly reflect the existence of a thick oceanic crust in the Iceland region, commonly related to hotspot activity. A weaker but positive elongated anomaly delineates the Mid-Atlantic Ridge south of Iceland in good correlation with a strong positive gravity anomaly (Sandwell & Smith 1994). Low-amplitude positive anomalies are located over the Azores High and King's Trough. The former correlates with geophysical and geochemical anomalies along the Mid-Atlantic Ridge (LeDouaran & Francheteau 1981). A positive anomaly is also seen on the satellite map over the Alpha Ridge in the Arctic Ocean which has been linked to the Iceland–Faroe Ridge presumed to have been formed by the same hotspot (e.g. Forsyth *et al.* 1986). The positive anomalies over Davis Strait and between Iceland and Greenland (Fig. 8a) are most likely related to hotspot-related volcanism. However, no consistent features are observed over other hotspot-related features such as the New England and Corner Seamounts, the Canary Island and Atlantis Meteor Seamount Complex, most likely due to their relatively smaller dimensions.

A positive magnetic anomaly is clearly identified over the Rockall Plateau. The plateau is a stretched microcontinent confirmed by the recovery of Precambrian (about 1.6 Ga) metamorphic granulites from drill holes (Roberts, Ardus & Dearnley 1973), the gravity and seismic surveys (Scrutton 1972), and continental reconstructions (Srivastava & Tapscott 1986; Srivastava & Roest 1989). Being surrounded by the oceanic lithosphere, the magnetic anomaly of the plateau provides a reasonable estimate of the bulk magnetization contrast, about 22 000 A, between the lithosphere of the plateau and that of the surrounding ocean (Toft & Arkani-Hamed 1993).

ACKNOWLEDGMENTS

This research was partially supported by the Natural Sciences and Engineering Research Council (NSERC) of Canada, Operating Grant OGP0041245 to JAH, and partly by the Atlantic Geoscience Centre. We would like to thank John LaBrecque and Doug Alsdorf for reviewing the paper and giving constructive comments. John LaBrecque kindly provided the computer program we used to calculate Malin's model. We gratefully acknowledge the contribution of all organizations and individuals who provided us with marine data, either directly or indirectly via the National Geophysical Data Center in Boulder, Colorado, and Tiku Ravat and his coworkers for allowing us to use their unpublished gridded Magsat data. We also thank P. Turner for the Xmgr software used to draw the plots in this paper.

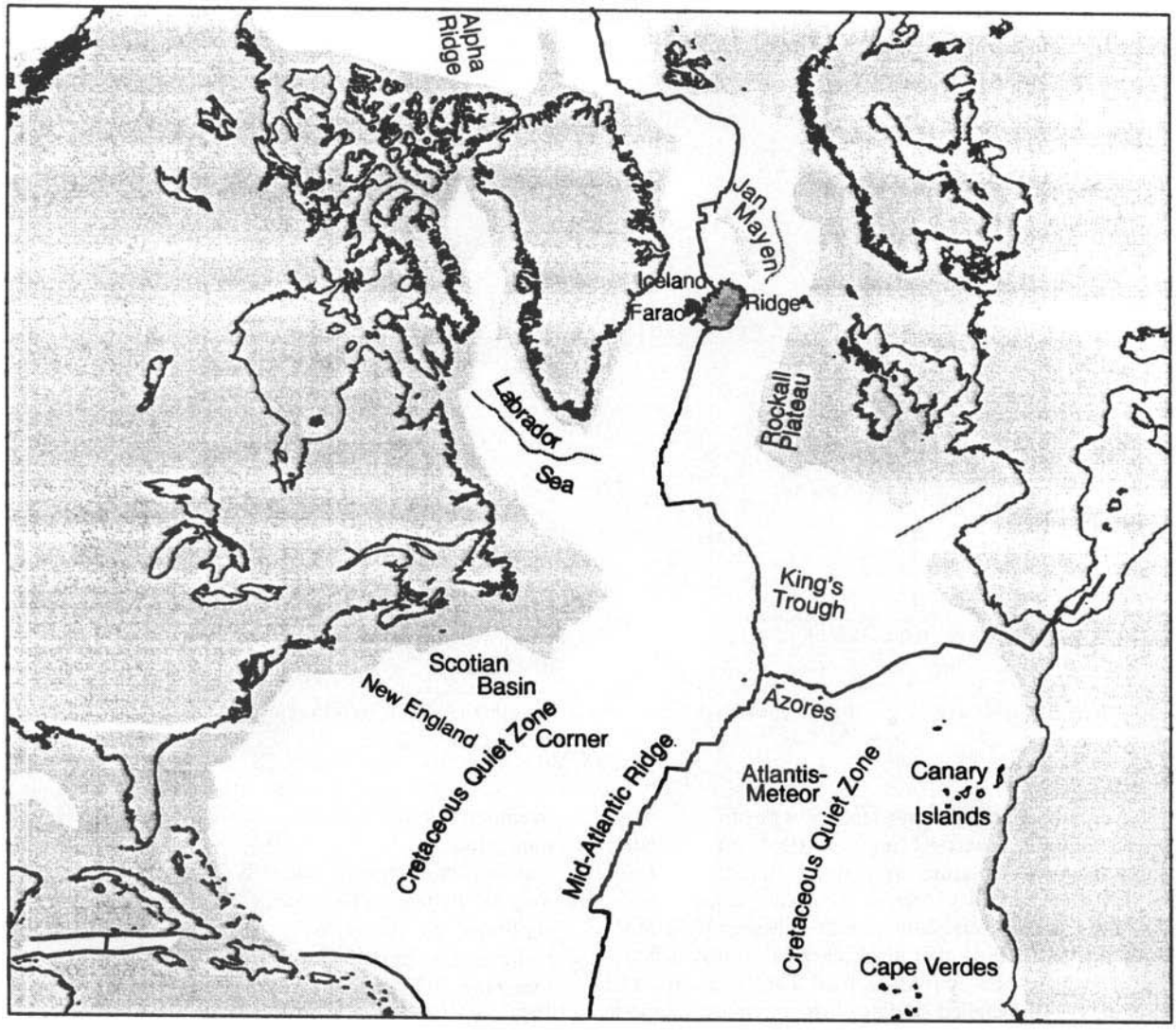

Figure 11. General tectonic framework for the North Atlantic Ocean and locations of geological features cited in the text. Heavy black lines represent active plate boundaries and heavy grey lines extinct spreading ridges in the Bay of Biscay, Labrador Sea and Aegir Ridge (Müller *et al.* 1993). Continental regions and land are shaded. For a summary of the references used to create the digital continent–ocean boundary, we refer to Müller & Roest (1992). Also shown are the general locations of the Cretaceous magnetic quiet zones.

REFERENCES

Arkani-Hamed, J., 1990. Magnetization of oceanic crust beneath the Labrador Sea, *J. geophys. Res.*, **95**, 7101–7110.

Arkani-Hamed, J., 1993. The bulk magnetization contrast across the ocean–continent boundary in the east coast of North America, *Geophys. J. Int.*, **115**, 152–158.

Arkani-Hamed, J. & Hinze, W.J., 1990. Limitations of the long-wavelength components of the North American magnetic anomaly map, *Geophysics*, **55**, 1577–1588.

Arkani-Hamed, J. & Strangway, D.S., 1986. Crustal magnetic susceptibility anomalies of lithosphere beneath the Eastern Europe and the Middle-East, *Geophysics*, **51**, 1711–1724.

Arkani-Hamed, J., Langel, R.A. & Purucker, M., 1994. Scalar magnetic anomaly maps of Earth derived from POGO and Magsat data, *J. geophys. Res.*, **99**, 24 075–24 090.

Bleil, U. & Petersen, N., 1983. Variations in magnetization intensity and low-temperature titanomagnetite oxidation of ocean floor basalts, *Nature*, **301**, 384–388.

Bradley, L.M. & Frey, H.V., 1991. Magsat magnetic anomaly contrast across Labrador Sea passive margins, *J. geophys. Res.*, **96**, 16 161–16 168.

Bullard, E.C. & Mason, R.G., 1961. The magnetic field astern of a ship, *Deep Sea Res.*, **8**, 20–27.

Cain, J.C., Wang, Z., Schmitz, D.R. & Mayer, J., 1989. The geomagnetic spectrum for 1980 and the core-crustal separation, *Geophys. J. Int.*, **97**, 443–447.

Cohen, Y. & Achache, J., 1990. New global vector magnetic anomaly maps derived from Magsat data, *J. geophys. Res.*, **95**, 10 783–10 800.

Coles, R.L., 1985. Magsat scalar magnetic anomalies at northern high latitudes, *J. geophys. Res.*, **90**, 2576–2582.

Counil, J.L., Cohen, Y. & Achache, J., 1991. The global continent-ocean magnetization contrasts, *Earth planet. Sci. Lett.*, **103**, 354–364.

Eldholm, O. & Grue, K., 1994. North Atlantic volcanic margins: dimensions and production rates, *J. geophys. Res.*, **99**, 2955–2968.

Forsyth, D.A., Asudeh, I., Green, A.G. & Jackson, H.R., 1986. Crustal structure of the North Alpha Ridge beneath the Arctic Ocean, *Nature*, **322**, 349–352.

Fullerton, L.G., Frey, H.V., Roark, J.H. & Thomas, H.H., 1989. Evidence for a remanent contribution in Magsat data from the

Cretaceous quiet zone in the South Atlantic, *Geophys. Res. Lett.*, **16**, 1085–1088.

Ghods, A., 1994. Negative magnetic anomalies at satellite altitude over passive marginal basins, *MSc Thesis*, Earth and Planetary Sciences, McGill University, Montreal, Canada.

Grauch, V.J.S., 1993. Limitations on digital filtering of the DNAG magnetic data set for the coterminous U.S., *Geophysics*, **58**, 1281–1296.

Haines, G.V., 1985. Magsat vertical field anomalies above 40°N from spherical cap harmonic analysis, *J. geophys. Res.*, **90**, 2593–2598.

Hood, P.J., Holroyd, M.T. & McGrath, P.H., 1979. Magnetic methods applied to base metal exploration, in *Geophysics and Geochemistry in the Search for Metallic Ores*, pp. 77–104, ed. Hood, P.J., Ministry of Supply and Services Canada, Ottawa, Ontario.

Jackson, H.R., Keen, C.E., Falconer, R.K.H. & Appleton, K.P., 1979. New geophysical evidence for seafloor spreading in central Baffin Bay, *Can. J. Earth. Sci.*, **16**, 2122–2135.

Kaiser, J.F., 1974. Nonrecursive digital filter design using the Io-sinh window function, *Proc. 1974 IEEE Int. Symp. Circuits and Systems*, 20–23.

LaBrecque, J.L. & Cande, S.C., 1984. Intermediate-wavelength magnetic anomalies over the central Pacific, *J. geophys. Res.*, **89**, 11 124–11 134.

LaBrecque, J.L. & Raymond, C.A., 1985. Seafloor spreading anomalies in the Magsat field, *J. geophys. Res.*, **90**, 2565–2575.

LaBrecque, J.L., Cande, S.C. & Jarrard, R.D., 1985. Intermediate-wavelength magnetic anomaly field of the North Pacific and possible source distributions, *J. geophys. Res.*, **90**, 2549–2564.

Langel, R.A., 1990. Global magnetic anomaly maps derived from POGO spacecraft data, *Phys. Earth planet. Inter.*, **62**, 208–230.

Langel, R.A. & Estes, R.H., 1985a. Large-scale, near-field magnetic fields from external sources and the corresponding induced internal field, *J. geophys. Res.*, **90**, 2487–2494.

Langel, R.A. & Estes, R.H., 1985b. The near-earth magnetic field at 1980 determined from Magsat data, *J. geophys. Res.*, **90**, 2495–2509.

LeDouaran, S. & Francheteau, J., 1981. Axial depth anomalies from 10° to 50° North along the Mid-Atlantic Ridge: correlation with other mantle properties, *Earth planet. Sci. Lett.*, **54**, 29–47.

Lincoln, J.V., 1967. Geomagnetic indices, in *Physics of Geomagnetic Phenomena*, pp. 67–100, eds Matsushita, S. & Campbell, W.H., Academic Press, New York.

Malin, S.R.C., 1973. Worldwide distribution of geomagnetic tides, *Phil. Trans. R. Soc. Lond.*, A, **274**, 551–594.

Mayhaud, P.N., 1980. Derivation, Meaning and Use of Geomagnetic Indices, *Am. geophys. Un, Monogr.* 22.

Müller, R.D. & Roest W.R. 1992. Fracture zones in the North Atlantic from combined Geosat and Seasat data, *J. geophys. Res.*, **97**, 3337–3350.

Müller, R.D., Roest, W.R., Royer, J.C., Gahagan, L. & Sclater, J.G., 1993. A digital age map of the ocean floor, *Scrips Institution of Oceanography Reference Series No. 93–30.*

Nakatsuka, T. & Ono, Y., 1984. Geomagnetic anomalies over the Japanese Islands region derived from MAGSAT data, *J. Geomagn. Geoelect.*, **36**, 455–462.

Naudy, H. & Dryer, H., 1968. Assai de filterage non-lineaire applique aux profils aeromagnetiques, *Geophys. Prospect.*, **16**, 171–178.

Ravat, D.N. & Hinze, W.J., 1993. Considerations of variations in ionospheric field effects in mapping equatorial lithospheric Magsat magnetic anomalies, *Geophys. J. Int.*, **113**, 387–398.

Ravat, D.N., Langel, R.A., Purucker, M., Arkani-Hamed, J. & Alsdorf, D., 1995. Vector and scalar Magsat magnetic anomaly maps for geologic interpretation, *J. geophys. Res.*, in press.

Rikitake, T., 1966. *Electromagnetism and The Earth's Interior*, pp. 154–198, Elsevier, New York.

Roberts, D.G., Ardus, D.A. & Dearnley, R., 1973. Precambrian rocks drilled on the Rockall Bank, *Nature Phys. Sci.*, **244**, 21–23.

Sandwell, D.T. & Smith, W.H.F., 1994. New global marine gravity map/grid based on stacked ERS-1, Geosat and Topex altimetry [abstract], *EOS, Trans. Am. geophys. Un.*, suppl., **75**, 321.

Scrutton, R.A., 1972. The crustal structure of Rockall plateau microcontinent, *Geophys. J. R. astr. Soc.*, **27**, 259–275.

Srivastava, S.P. & Roest, W.R., 1989. Seafloor spreading history II–VI, in *East Coast Basin Atlas Series: Labrador Sea*, pp. 100–109, coordinator, Bell, J.S., Geological Survey of Canada, Atlantic Geoscience Centre, scale 1:2 000 000.

Srivastava, S.P. & Tapscott, C.R., 1986. Plate kinematics of the North Atlantic, in *The Geology of North America, vol. M, The Western North Atlantic Region*, pp. 379–403, eds Vogt, P.R. & Tuckolke, B.E., Geological Society of America, Boulder, CO.

Toft, P.B. & Arkani-Hamed, J., 1992. Magnetization of the Pacific ocean lithosphere deduced from Magsat data, *J. geophys. Res.*, **97**, 4387–4406.

Toft, P.B. & Arkani-Hamed, J., 1993. Induced magnetization of the oceanic lithosphere and ocean–continent magnetization contrast inferred from Magsat anomalies, *J. geophys. Res.*, **98**, 6267–6282.

Verhoef, J. & Macnab, R., 1989. Definitive Magnetic Reference Field (DGRF) evaluation based on marine magnetic anomalies, *Phys. Earth planet. Inter.*, **54**, 332–339.

Verhoef, J., Roest, W.R., Macnab, R., Arkani-Hamed, J. & members of the project team, 1994. A compilation of magnetic observations from the Arctic and North Atlantic Oceans and adjacent land areas, *Society of Exploration Geophysicists International Exposition and 64th Annual Meeting*, Expanded Abstract, 853–855.

Von Frese, R.R.B., Hinze, W.J., Sexton, J.L. & Braile, L.W., 1982. Verifications of the crustal components in satellite magnetic data, *Geophys. Res. Lett.*, **9**, 293–295.

White, R.S. & McKenzie, D., 1989. Magmatism at rift zones: the generation of volcanic continental margins and flood basalts, *J. geophys. Res.*, **94**, 7685–7729.